ISSN 1674-1056
http://cpb.iphy.ac.cn
http://iopscience.iop.org/cpb
中国物理 B
Chinese Physics
中国物理 Chinese Physics B

High uniformity and forming-free ZnO-based transparent RRAM with HfO_x inserting layer

Shi-Jian Wu(吴仕剑), Fang Wang(王芳), Zhi-Chao Zhang(张志超), Yi Li(李毅), Ye-Mei Han(韩叶梅), Zheng-Chun Yang(杨正春), Jin-Shi Zhao(赵金石), Kai-Liang Zhang(张楷亮)

Citation: Chin. Phys. B . 2018, 27(8): 087701. **doi:** 10.1088/1674-1056/27/8/087701

Journal homepage: http://cpb.iphy.ac.cn; http://iopscience.iop.org/cpb

What follows is a list of articles you may be interested in

Effect of O-O bonds on p-type conductivity in Ag-doped ZnO twin grain boundaries

Jingjing Wu(吴静静), Xin Tang(唐鑫), Fei Long(龙飞), Biyu Tang(唐壁玉)

Chin. Phys. B . 2018, 27(5): 057701. **doi:** 10.1088/1674-1056/27/5/057701

Propagations of Rayleigh and Love waves in ZnO films/glass substrates analyzed by three-dimensional finite element method

Yan Wang(王艳), Ying-Cai Xie(谢英才), Shu-Yi Zhang(张淑仪), Xiao-Dong Lan(兰晓东)

Chin. Phys. B . 2017, 26(8): 087703. **doi:** 10.1088/1674-1056/26/8/087703

ZnO-based deep-ultraviolet light-emitting devices

Ying-Jie Lu(卢英杰), Zhi-Feng Shi(史志锋), Chong-Xin Shan(单崇新), De-Zhen Shen(申德振)

Chin. Phys. B . 2017, 26(4): 047703. **doi:** 10.1088/1674-1056/26/4/047703

Recent progress of the native defects and p-type doping of zinc oxide

Kun Tang(汤琨), Shu-Lin Gu(顾书林), Jian-Dong Ye(叶建东), Shun-Ming Zhu(朱顺明), Rong Zhang(张荣), You-Dou Zheng(郑有炓)

Chin. Phys. B . 2017, 26(4): 047702. **doi:** 10.1088/1674-1056/26/4/047702

Comparative research on the optical properties of three surface patterning ZnO ordered arrays

Hou Kai, Zhu Ya-Bin, Qiao Lu

Chin. Phys. B . 2015, 24(12): 127703. **doi:** 10.1088/1674-1056/24/12/127703

High uniformity and forming-free ZnO-based transparent RRAM with HfO_x inserting layer*

Shi-Jian Wu(吴仕剑), Fang Wang(王芳)†, Zhi-Chao Zhang(张志超), Yi Li(李毅), Ye-Mei Han(韩叶梅), Zheng-Chun Yang(杨正春), Jin-Shi Zhao(赵金石), and Kai-Liang Zhang(张楷亮)‡

School of Electronics Information Engineering, Tianjin Key Laboratory of Film Electronic & Communication Devices, Tianjin University of Technology, Tianjin 300384, *China*

(Received 24 April 2018; revised manuscript received 30 May 2018; published online 10 July 2018)

The impacts of HfO_x inserting layer thickness on the electrical properties of the ZnO-based transparent resistance random access memory (TRRAM) device were investigated in this paper. The bipolar resistive switching behavior of a single ZnO film and bilayer HfO_x/ZnO films as active layers for TRRAM devices was demonstrated. It was revealed that the bilayer TRRAM device with a 10-nm HfO_x inserted layer had a more stable resistive switching behavior than other devices including the single layer device, as well as being forming free, and the transmittance was more than 80% in the visible region. For the HfO_x/ZnO devices, the current conduction behavior was dominated by the space-charge-limited current mechanism in the low resistive state (LRS) and Schottky emission in the high resistive state (HRS), while the mechanism for single layer devices was controlled by ohmic conduction in the LRS and Poole–Frenkel emission in the HRS.

Keywords: transparent resistive random access memory (TRRAM), HfO_x inserting layer, uniformity, forming-free

PACS: 77.55.hf, 85.35.–p, 85.30.–z **DOI:** 10.1088/1674-1056/27/8/087701

1. Introduction

Resistive random access memory (RRAM) is considered as the best potential candidate for the next generation of non-volatile memory because of its simple structure, good scalability, fast write/read speed, and low power consumption.[1,2] With the emergence of transparent electronics, transparent RRAM (TRRAM) has many prospective applications in invisible electronics based on integration of wide-bandgap semiconductors. It has attracted many researchers to develop see-through memory units instead of traditional silicon-based data storage devices. Recently, many different materials, such as ZnO, TiO_2, SiO_x, HfO_2, IGZO, AlN, and egg albumen, have been discovered as effective active layers for TRRAM.[3–9] Transition metal oxides have great advantages not only in compatibility with CMOS processes, but also in their thermal and chemical stability, as well as high transparency in the visible region. ZnO has been considered as an excellent active layer for RRAM due to good performance of resistive switching properties such as the coexistence of unipolar and bipolar switching behaviors, transparency, and flexible application. However, variation in critical switching parameters and power consumption remain challenges in single layer ZnO films for potential TRRAM applications.[3,10,11] Multilayering is one effective way to improve the resistive switching behavior.[12–17] In this paper, the single layer TRRAM device (SL-TRRAM) with ITO/ZnO/ITO structure and effects of inserting layer thickness of HfO_x film on resistance switching properties of bilayer TRRAM device (BL-TRRAM) were investigated. In addition to being forming-free and having a lower reset current, the BL-TRRAM devices with 10-nm HfO_x thickness had better uniformity compared to SL-TRRAM. Moreover, the average transmittance of the devices was above 80% in the visible range. The switching mechanism of the SL-TRRAM device in the low resistive state (LRS) and high resistive state (HRS) was consistent with ohmic conduction and Poole–Frenkel emission, while the BL-TRRAM was controlled by the space-charge-limited current (SCLC) and Schottky emission mechanism.

2. Experiment

A 50-nm ZnO thin film was deposited by radio-frequency (RF) magnetron sputtering using a ZnO ceramic target on a commercial ITO-coated glass substrate in argon-oxygen (32:8) at 200 °C. For the bilayer TRRAM, HfO_x films with different thicknesses (5 nm, 10 nm, and 15 nm) were sputtered on ZnO film in an ambient environment of Ar (36 sccm) and O_2 (6 sccm). 150-nm ITO was deposited as the top electrode (TE) in an Ar environment with a metal mask 300 μm

*Project supported by the National Key Research and Development Program of China (Grant No. 2017yfb0405600), the National Natural Science Foundation of China (Grant Nos. 61404091, 61274113, 61505144, 51502203, and 51502204), and the Natural Science Foundation of Tianjin City (Grant Nos. 17JCYBJC16100 and 17JCZDJC31700).

†Corresponding author. E-mail: fwang75@163.com

‡Corresponding author. E-mail: kailiang_zhang@163.com

© 2018 Chinese Physical Society and IOP Publishing Ltd

in diameter. Optical transmittance of the device was measured using a Lambda 750 UV/VIS spectrophotometer. The crystal structure and surface morphology of the ZnO film and HfO_x film were analyzed by x-ray diffraction (XRD) and atomic force microscopy (AFM), respectively. The resistive switching characteristics of TRRAM devices were measured using an Agilent B1500 semiconductor parameter analyzer. The bias was applied on the TE while the bottom electrode (BE) was grounded.

3. Results and discussion

As shown in Fig. 1(a), the SL-TRRAM device displayed a typical bipolar resistance switching, in which the set and reset processes occurred in the positive and negative bias regions, respectively. Activation of the TRRAM devices required a forming process, as shown in the inset of Fig. 1(a), in which the forming voltage was about −1.4 V. After the initial forming process, the RRAM devices changed to a low resistance state and then the voltage was swept as 0 V→4.0 V→0 V→−3.0 V→0 V. The operation current was about 50 mA. The operation voltage fluctuated widely while repeating the reset and set processes over 20 cycles. Statistical analysis found that the set voltage was spread between −0.84 V and 0.55 V and the reset voltage had a larger spread between 2.03 V and 2.72 V. To study the device endurance, one of the fundamental challenges in nonvolatile memory devices, the LRS and HRS were measured at a bias voltage of −0.1 V for different switching cycles as shown in Fig. 1(b). Resistances in LRS at different switching cycles up to 200 were very steady at around 40 Ω, while in HRS the resistance decayed from 6 kΩ to 2 kΩ. Similar attenuation in the HRS with switching cycles has also been found in the previous research[18] and can be explained in terms of continuous depletion of oxygen ions stocked in the electrode layer during reset transition. The lack of oxygen ions reduced the probability of recombination of oxygen vacancies, thus caused the insufficient reset and reduction of the HRS resistance.

There were major obstacles in using the ZnO single layer for practical applications, including non-uniformity in the distribution of operation voltage and high operation current. Therefore, bilayer HfO_x–ZnO TRRAM devices with three different thicknesses of inserting layer HfO_x film were fabricated to improve the resistive switching behavior. The reset current decreased as the inserting layer thickness increased from 5 nm to 10 nm, while there was no significant change from 10 nm to 15 nm, as shown in Fig. 2(a). In addition, the *I*–*V* curve showed that the operation current was reduced from mA to μA, more than 10^3 times less than that with the SL-TRRAM device, indicating low power consumption. Furthermore, the endurance characteristics of devices with three different thicknesses were tested, as shown in Figs. 2(b)–2(d). The result indicated that the device with the 10-nm HfO_x film exhibited a stable and high resistance ratio between HRS and LRS for 200 cycles, while there was high fluctuation and degradation of the resistance ratio (below 10 for 50 cycles) in HRS and LRS for the devices with 5 nm and 15 nm HfO_x films, which means the device performance was invalid. The improvement of endurance failure for the 10-nm sample could be regarded as the electrode generated more O^{2-} to recover the reduced R_{HRS} with higher operating voltages.[18]

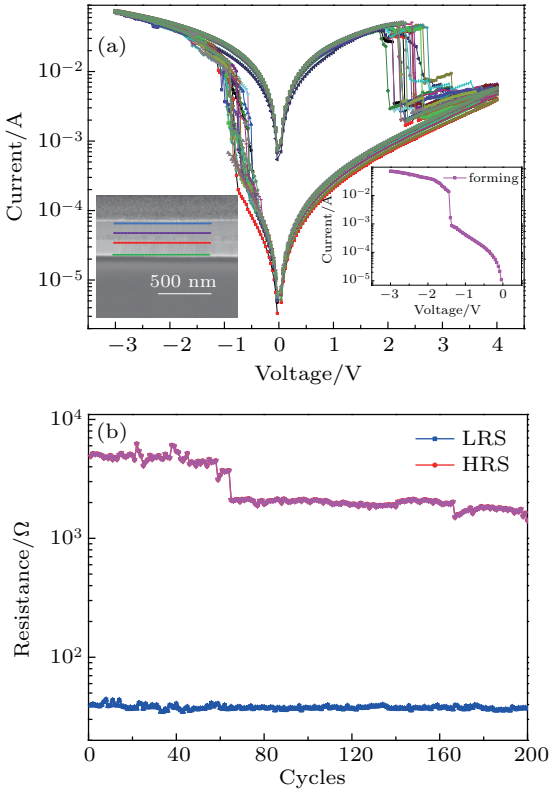


Fig. 1. (color online) (a) *I*–*V* characteristic, and insert is a cross-sectional image of the ITO/ZnO/ITO structure and forming process; (b) endurance of the SL-TRRAM.

Because of its relatively outstanding performance, the device with 10-nm thick HfO_x inserting film was further studied. As shown in Fig. 3(a), the subsequent cycles are almost coincident with the first cycle (red line), indicating that the device was electroforming-free. Meanwhile, the reset voltages were uniformly distributed close to 3 V over 20 cycles, as shown in Fig. 3(b), which was much better than the SL-TRRAM devices. Figure 3(c) showed that the resistance in the HRS for the BL-TRRAM device fluctuated less than the SL-TRRAM. Figure 3(d) exhibited variation in HRS and LRS with time for the BL-TRRAM device at 85 °C. After 10^4 s, there was no obvious degradation observed in HRS or LRS. The results showed a remarkably reliable performance of the TRRAM devices for nonvolatile memory application.

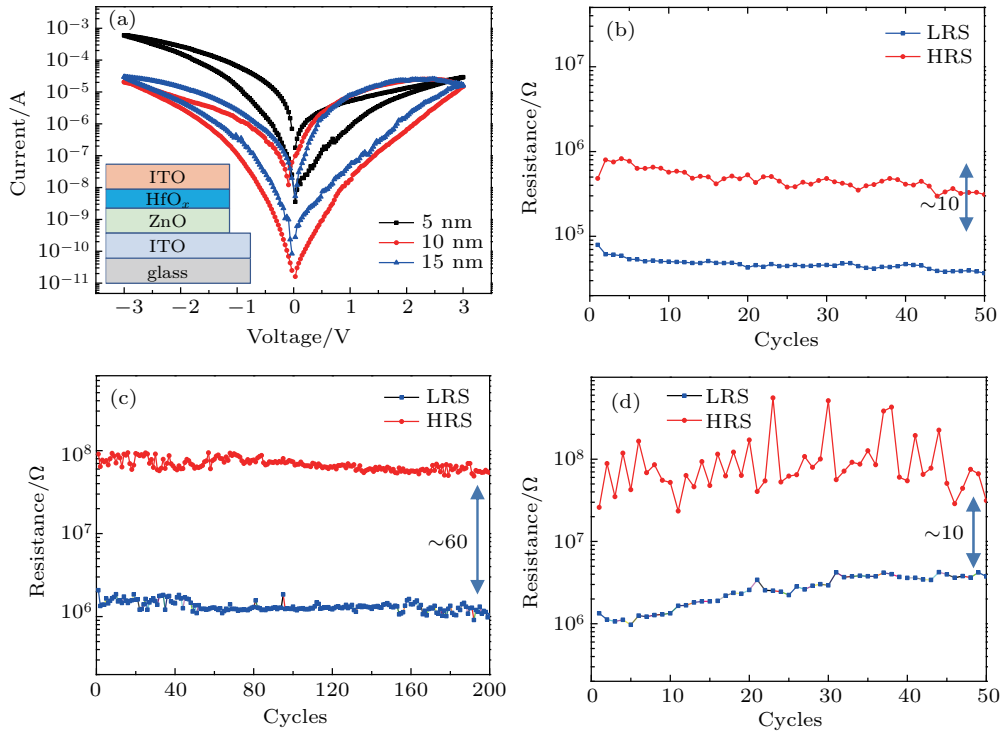


Fig. 2. (color online) ITO/HfO_x/ZnO/ITO structure devices. (a) *I*–*V* characteristics; (b) endurance of different HfO_x thicknesses of 5 nm, (c) 10 nm, and (d) 15 nm, and the double arrows and numbers in panels (b), (c), and (d) indicate the resistance ratio between HRS and LRS.

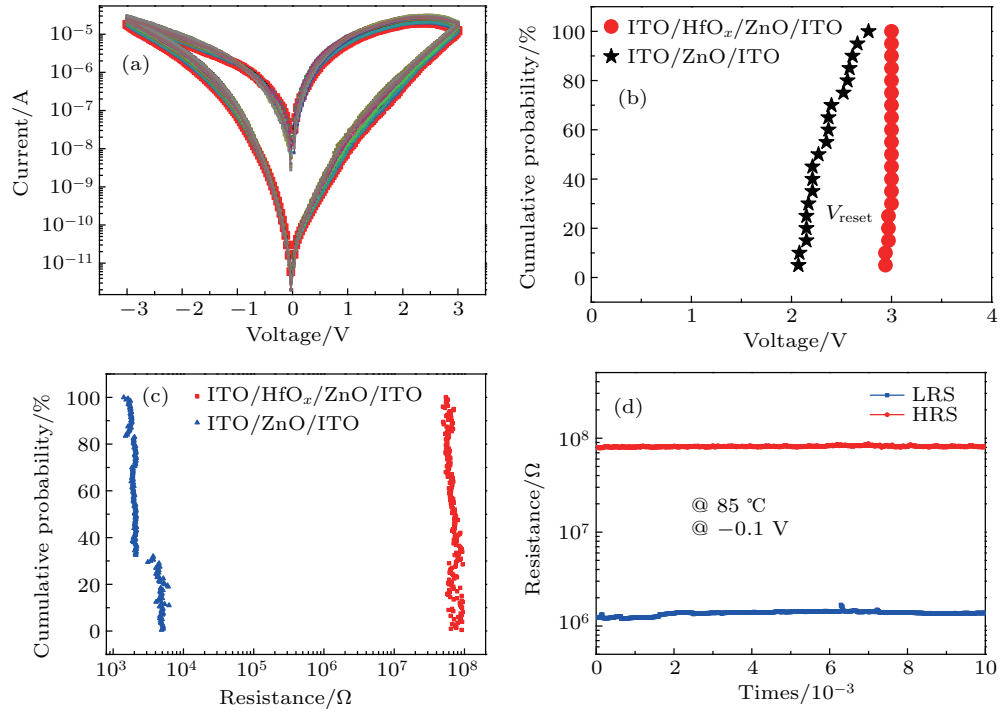


Fig. 3. (color online) 10 nm-HfO_x bilayer TRRAM. (a) *I*–*V* curves up to 20 cycles; the cumulative distributions of (b) the operating voltages, (c) resistance in the HRS for SL-RRAM and BL-RRAM, and (d) retention.

Next, the surface morphology of the ZnO and HfO_x films and crystal structure of the HfO_x film deposited on ITO/glass substrate were analyzed using AFM and XRD, respectively, the results of which are shown in Fig. 4. The RMS roughnesses of the ZnO and HfO_x thin films were 2.57 nm and 2.94 nm, respectively, which suggests that the thin films were relatively flat. Figure 4(c) shows the crystalline structure of the ZnO film with (002)-orientation; the HfO_x film had no significant orientation. Figure 4(d) displayed the transmission spectra of the fabricated SL-TRRAM and BL-TRRAM devices. The devices had a high transmittance around 80% in the visible region, indicating the notable transparency property and potential application for transparent display.

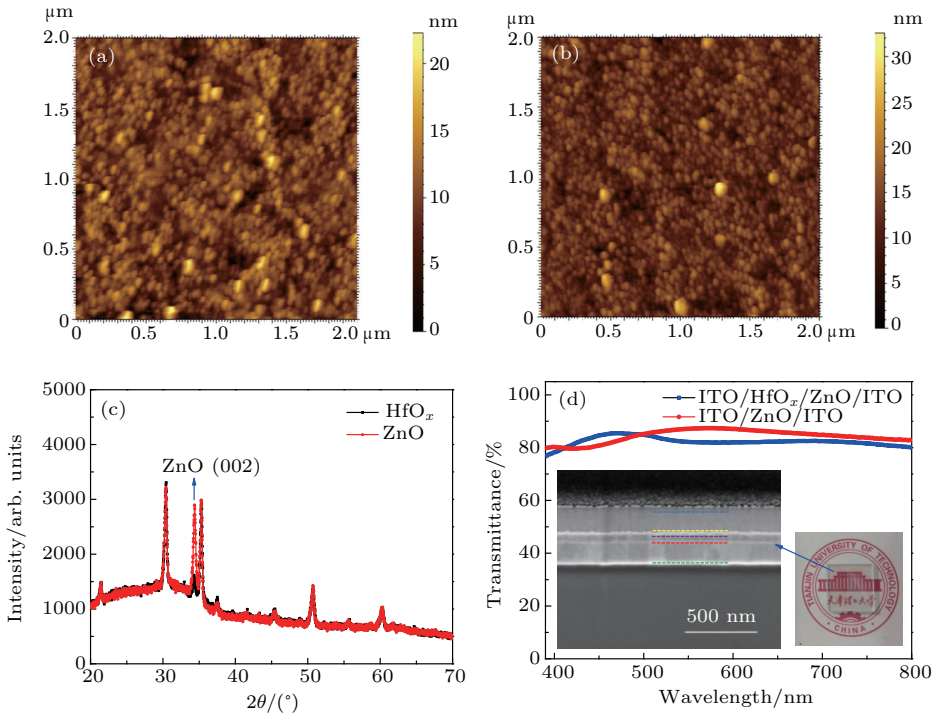


Fig. 4. (color online) (a) AFM image of ZnO film; (b) AFM image of 10-nm HfO$_x$ film; (c) XRD spectra of the ZnO and HfO$_x$ film deposited on ITO/glass substrate; (d) optical transmission spectra of the SL-TRRAM and BL-TRRAM devices, and the inset is cross-sectional image and photograph of the bilayer device placed onto a background log.

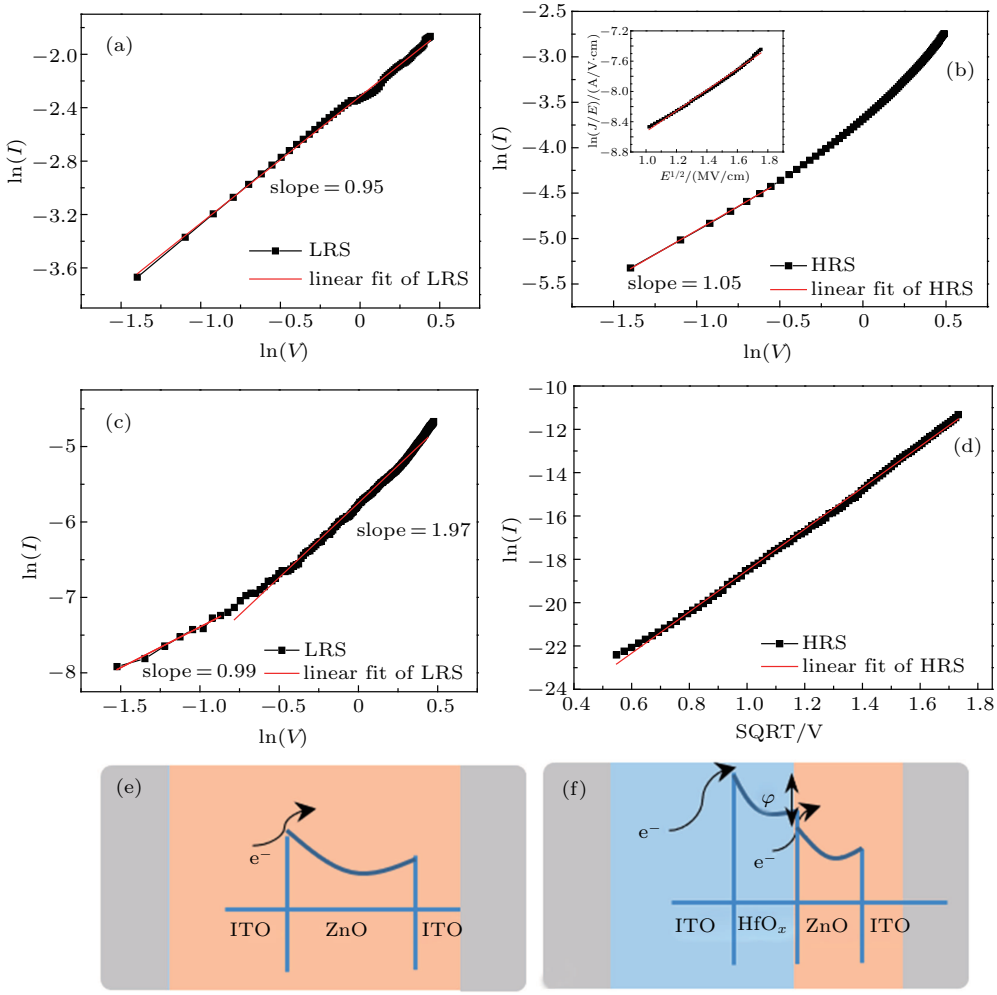


Fig. 5. (color online) Double logarithmic plot and linear fitting of *I*–*V* curve (a) in the LRS and (b) in the HRS for SL-TRRAM; (c) in the LRS and (d) in the HRS for BL-TRRAM. Schematic diagrams of band structure for (e) SL-TRRAM device and (f) BL-RRAM device.

To clarify the conduction mechanisms of the devices, I–V curves for both LRS and HRS states were fitted to various electrical conduction mechanisms with double logarithmic curves. For the SL-TRRAM, as shown in Figs. 5(a) and 5(b), the linear fittings of $\ln(I)$ versus $\ln(V)$ and the $\ln(J/E)$ versus $E^{0.5}$ (J is current density and E is electric field) signified an Ohm's law dominant conduction in the LRS and Ohm's law at a low voltage region and Poole–Frenkel emission-governed conduction in the high voltage region in the HRS.[3] The mechanism for the resistance switching was based on the formation and rupture of conduction filaments due to the migration of oxygen ions and filling of the traps by electrons (as shown in Fig. 5(e)). However, the double logarithmic I–V curves of LRS and HRS for BL-TRRAM, as shown in Figs. 5(c) and 5(d), respectively, suggest that the SCLC mechanism accounts for the current conduction at LRS and that HRS has Schottky-emission conduction.

Due to the high Gibbs free energy of HfO_x thin films, the oxygen ions in ZnO migrate into HfO_x, making HfO_x less oxygen-deficient but more insulative. Moreover, because of the broken chemical bond of ZnO, free oxygen ions could be generated with the increased electric-field, and then migrate into HfO_x in the HRS, leading to enhanced conductivity of ZnO and insulation of HfO_x. Hence, electron transportation from the bottom electrode to the top electrode must overcome the barrier at the HfO_x/ZnO interface, as shown in Fig. 5(f), which is consistent with the Schottky emission mechanism.[19] The operating current of the device substantially degrades because the resistance is higher in the devices as the thickness of HfO_x film increases due to the modulation of the barrier.[17] When the electric field is further increased to finish the set process, oxygen vacancies would be generated in HfO_x film, but would be not sufficient for direct electron transport between ZnO and HfO_x. The intrinsic defect, especially oxygen vacancy defects, is filled with the carriers which are injected with an increased electrostatic potential gradient.[20] Therefore, space-charge-limited current conduction is appropriate for the LRS. The uniformity of the BL-TRRAM device is improved because of the lack of randomness of the conduction filaments and the resistance switching change from ionic to electronic due to the HfO_x film.[21]

4. Conclusion and perspectives

In summary, the performance of SL-TRRAM and BL-TRRM devices were demonstrated in this paper. Both of the devices had a high transmittance above 80% in the visible region. The BL-TRRAM device with 10-nm-HfO_x thickness had more stable and uniform resistive switching behaviors than SL-TRRAM and was forming-free, while SL-TRRAM required a forming process. The conduction mechanisms of LRS and HRS are consistent with Ohmic conduction and Poole–Frenkel emission for SL-TRRAM, and SCLC and Schottky emission for BL-TRRAM, respectively. The results of this study indicate that the BL-TRRAM device has great potential for use in transparent memory devices.

References

[1] Lei X Y, Liu H X, Gao H X, Yang H N, Wang G M, Long S B, Ma X H and Liu M 2014 *Chin. Phys. B* **23** 117305

[2] Jiang R, Du X H, Han Y Z and Sun W D 2015 *Acta Phys. Sin.* **64** 207302 (in Chinese)

[3] Seo M S, Park J W, Lim K S, Yang J H and Kang S J 2008 *Appl. Phys. Lett.* **93** 223505

[4] Meng Y, Zhang P J, Liu Z Y, Liao Z L, Pan X Y, Liang X J, Zhao H W and Chen D M 2010 *Chin. Phys. B* **19** 037304

[5] Yang P J, Jou S and Chiu C C 2014 *Jpn. J. Appl. Phys.* **53** 075801

[6] Chen K H, Chang K C, Chang T C Chang T C, Tsai T M, Liang S P, Young T F, Syu Y E and Sze S M 2016 *Nanoscale Res. Lett.* **11** 224

[7] Ye C, Wu J J, Pan C H, Tsai T M, Chang K C, Wu H Q, Deng Ni and Qian H 2017 *RSC Adv.* **7** 11585

[8] Ho C H, Duran R, Jose R, Yang P K, Lee C P, Tsai, M L, Kang C F and He J H 2017 *Sci. Rep.* **7** 44429

[9] Zhu J X, Zhou W L, Wang Z Q, Xu H Y, Lin Y, Liu W Z, Ma J G and Liu Y C 2017 *RSC Adv.* **7** 32114

[10] Ma H L, Wang Z Q, Xu H Y, Zhang L, Zhao X N, Han S M, Ma J G and Liu Y C 2016 *Chin. Phys. B* **25** 127303

[11] Kim K Y, Shim E L and Choi Y J 2016 *J. Nanosci. Nanotechnol.* **16** 10303

[12] Pang H and Deng N 2014 *Chin. Phys. Lett.* **31** 107303

[13] Jiang R, Han Z Y and Du X H 2016 *Microelectronics Reliability* **63** 37

[14] Zhang K L, Sun K, Wang F, Han Y M, Jiang Z Z, Zhao J S, Wang B L, Zhang H Z, Jian X C and Wong H S P 2015 *IEEE Electron Dev. Lett.* **36** 1018

[15] Jiang R, Wu Z R, Han Z Y and Jung H S 2016 *Chin. Phys. B* **25** 106803

[16] Lai Y F, Chen F, Zeng Z C, Lin P J, Shu Y and Yu J L 2017 *Chin. Phys. B* **26** 087305

[17] Su S, Jian X C, Wang F, Han Y M, Tian Y X and Wang X Y 2016 *Chin. Phys. B* **25** 107302

[18] Chen B, Lu Y, Gao B, Fu Y H, Zhang F F, Huang P, Chen Y S, Liu L F, Liu X Y, Kang J F, Wang Y Y, Fang Z, Yu H Y, Li X, Wang X P, Singh N, Lo G Q and Kwong D L 2011 *International Electron Devices Meeting* **11** 283

[19] Lai Y F, Zeng Z C, Liao C H, Cheng S Y, Yu J L, Zheng Q and Lin P J 2016 *Appl. Phys. Lett.* **109** 063501

[20] Wei C C, Wang H, Xu J W, Zhang X W, Yang L and Chen Q S 2015 *J. Synth. Cryst.* **44** 649

[21] Shao X L, Zhou L W, Yoon K J, Jiang H, Zhao J S, Zhang K L, Yoo S and Hwang C S 2015 *Nanoscale* **7** 11063